Vacuum 204 (2022) 111331

Contents lists available at ScienceDirect

Vacuum

journal homepage: www.elsevier.com/locate/vacuum

Plasma diagnostics and film growth of multicomponent nitride thin films with magnetic-field-assisted-dc magnetron sputtering

Smita G. Rao *, Rui Shu, Robert Boyd, Arnaud le Febvrier, Per Eklund

Department of Physics, Chemistry, and Biology (IFM), Linköping University, 581 83, Linköping, Sweden

ARTICLE INFO

Keywords:
Plasma diagnostics
Multicomponent thin film
Magnetron sputtering
Nitrides
High entropy alloy

ABSTRACT

During direct current magnetron sputtering (dcMS) of thin films, the ion energy and flux are complex parameters that influence thin film growth and can be exploited to tailor their properties. The ion energy is generally controlled by the bias voltage applied at the substrate. The ion flux density however is controlled by more complex mechanisms.

In this study, we look into magnetic-field-assisted dcMs, where a magnetic field applied in the deposition chamber by use of a solenoid coil at the substrate position, influences the energetic bombardment by Ar ions during deposition. Using this technique, CrFeCoNi multicomponent nitride thin films were grown on Si(100) substrates by varying the bias voltage and magnetic field systematically. Plasma diagnostics were performed by a Langmuir wire probe and a flat probe. On interpreting the data from the current-voltage curves it was confirmed that the ion flux at the substrate increased with increasing coil magnetic field with ion energies corresponding to the applied bias. The increased ion flux assisted by the magnetic field produced by the solenoid coil aids in the stabilization of NaCl B1 crystal structure without introducing Ar ion implantation.

1. Introduction

Among the many methods available to alter growth kinetics in sputter-deposition processes, ion-assisted direct current magnetron sputtering (dcMS) can be used to alter the film's microstructure and properties by bombardment with energetic ions (typically Ar^+) and higher ion-flux conditions than a regular sputter-deposition process. While the energy of the bombarding ions is normally controlled by the applied bias voltage to the substrate [1], the flux of ions can be significantly increased either by using an additional ion source, or by extracting and accelerating the existing ions in the plasma [2–5].

In this work, we focus on magnetic-field-assisted *dc* magnetron sputtering. This technique makes use of a magnetic field produced by a solenoid coil placed around the substrate to influence the energy and flux of Ar ions close to the substrate. Studies have shown the influence of ion energy and flux on the resulting film growth and microstructure for sputter deposition of Mo, Ti and TiN films [6–8]. When growing binary metallic films, the effects of increased Ar ion bombardment are relatively straightforward, the increased flux and energy of Ar ions both can lead to densification of the growing film along with a change in texture [9]. In the case of ceramic materials such as nitrides, the effects can be more complex. A study where single crystal TiN films were grown in excess N and pure N_2 discharges reported the formation of nanometer-sized N_2 bubbles [10]. This is a result of inhibited desorption and segregation of N ions during high bias voltage assisted growth.

These studies serve as a foundation for understanding film growth in much more complex systems such as multicomponent materials. This class of materials is gaining popularity for their mechanical, electrical, electrochemical, and irradiation-resistant properties [11–13]. Here, we focus on understanding the effect of ion energy and flux on the growth of CrFeCoNi multicomponent nitride thin films.

2. Experimental details

Plasma diagnostics and thin-film deposition were carried out in an unbalanced magnetron sputtering system equipped with a solenoid coil. A schematic of the ultra-high vacuum sputtering system can be found in the supplementary information (Fig. S1) however, details of the system are described elsewhere [14]. In brief, the system consists of four magnetron assemblies placed ~13 cm from and at an angle of 30° to the substrate holder. The magnetic fields of adjacent magnetron assemblies are coupled. The solenoid coil placed around the substrate

* Corresponding author.
E-mail address: smita.gangaprasad.rao@liu.se (S.G. Rao).

https://doi.org/10.1016/j.vacuum.2022.111331
Received 10 March 2022; Received in revised form 13 June 2022; Accepted 8 July 2022
Available online 13 July 2022

holder/sample stage is a Kapton-insulated Cu wire wound around a stainless-steel frame with an in-built cooling system. The solenoid coil is operated by setting the coil current to produce a magnetic field between 0 and 8.5 mT. A plot of the magnetic field produced by the coil as a function of the current can be found in Ref. [14]. When turned on, the coil assists in the deposition processes by coupling the outer pole of one pair of opposing magnetrons. The magnetic field lines of the outer poles of the active magnetrons are directed towards the substrate and not towards the neighboring magnetrons. Plasma diagnostics were carried out with the same target power and processes parameters used for film growth mentioned later.

A Langmuir wire probe and flat probe were used for obtaining the current (I) – voltage (V) characteristics. The Langmuir wire probe consisted of an 0.5-mm-diameter and 3 mm long tungsten wire shielded within ceramic tubes. These homemade probes were inserted through the load-lock chamber and positioned at the location of the substrate holder. The substrate table was always at the same potential as the probe during the study. The plasma potential (V_p) was determined from I–V curves in the electron-current region obtained from the Langmuir wire probe. Current measurements were made in the range from −70 to +15 V of applied bias potential.

The floating potential (V_f) was determined from the I–V curves in the ion-saturation region obtained from the flat probe. The flat probe was designed in a manner where the I–V characteristics could be recorded at five different positions on a circular, 50.8-mm (2-inch) diameter, stainless-steel plate. The data presented in this work was recorded from the center position of the probe/electrode. A schematic view of the flat probe is provided in the supplementary information (Fig. S2). A LabView program was used to collect data and obtain the I–V curves [15].

(CrFeCoNi)N films were grown on 50.8-mm (2-inch) diameter silicon (100) substrates. The base pressure was 3×10^{-7} Pa. Depositions and plasma diagnostics were carried out in an Ar + N_2 atmosphere (working pressure, 0.53 Pa), where the relative nitrogen gas flow $(F_{N_2}) = 70\%$ which can be defined as,

$$F_{N_2} = \frac{f_{N_2}}{\left(f_{N_2} + f_{Ar}\right)} \tag{1}$$

where, f_{N_2} is the nitrogen partial flow, f_{Ar} is the argon partial flow. A relative nitrogen gas flow of 70% was chosen as it resulted in a stochiometric nitride thin film. A compound target with composition $Cr_{24}Fe_{32}Co_{24}Ni_{20}$ (provided by Plansee, Composite Materials GmbH) target thickness 3 mm, and 50.8 mm (2-inch) diameter was sputtered with a constant target power of 100 W.

θ-2θ X-ray diffraction (XRD) patterns were obtained using a PANalytical X'Pert PRO diffractometer operated using Cu-Kα radiation (λ = 1.54060 Å) at a voltage of 45 kV and current of 40 mA. Scans were carried out in the Bragg-Brentano configuration.

Scanning electron microscope (SEM, Sigma) was used for imaging using the in-lens detector with an acceleration voltage of 2 kV. (Scanning) transmission electron microscopy [(S)TEM] was carried out on the samples in a FEI Tecnai G2 TF 20 UT instrument operated at 200 kV. Electron transparent cross-section samples were prepared by focused ion beam (FIB) in a Zeiss Neon 40 dual beam workstation using 30 kV/2 nA Ga^+ ion. A layer of platinum was deposited on the area to be milled in order to protect it the sample from the milling process. The cross sections were extracted by lift-out technique. A final thinning down and polishing were done using 200 pA and 50 pA currents.

The elemental composition of the films in series 2 was determined by time-of-flight elastic recoil detection analysis (ToF-ERDA). Measurements were carried out at Uppsala University (Sweden) in a 5 MV NEC-5SDH-2 Pelletron Tandem accelerator. ToF-ERDA results were obtained at a 45° recoil angle between the 36 MeV $^{127}I^{8+}$ primary beam incident at 67.5° and a gas ionization chamber detector. Depth profiles of the elemental composition were acquired from ToF-ERDA time and energy coincidence spectra with the Potku 2.0 software package [16]. The results obtained gave an estimate of the overall metal content, nitrogen, oxygen, and argon contents. The composition was extracted from a 50–100 nm range to avoid the top 5–10 nm which showed the presence of surface oxidation.

Table 1
Deposition parameters of (CrFeCoNi)N multilayered and monolithic films grown in series 1 and series 2 respectively.

Series 1: ion-energy controlled growth		
Deposition temperature (°C)	Bias voltage (V) varied	Magnetic field (mT)
RT	−40 → −130	4.5
300		

Table 2
Deposition parameters of (CrFeCoNi)N multilayered and monolithic films grown in series 1 and series 2 respectively.

Series 2: ion-flux controlled growth		
Deposition temperature (°C)	Bias voltage (V)	Magnetic field (mT)
RT	−100	0
300		2.5
		4.5
		6.5

Along with the plasma study, two film growth series were carried out. The first one (**series 1**: ion-energy controlled growth) where the coil magnetic field was set at 4.5 mT while the bias was varied from −40 to −130 V and the second (**series 2**: ion-flux density-controlled growth) where the bias voltage was set at −100 V and the coil magnetic field was varied from 0 to 6.5 mT. Table 1 and 2 list out the deposition parameters of the two series.

3. Results and discussion

As mentioned above, the work is split into three sections as shown in Fig. 1. Results from these three sections are presented in the same order as in the figure.

3.1. Plasma study

The I–V characteristics obtained from the flat probe for each magnetic field are shown in Fig. 2a. Similarly, I–V characteristics were obtained from the Langmuir wire probe as well (Fig. 2b). The floating potential and plasma potentials for each coil magnetic field were calculated from these I–V curves. Increasing the magnetic field from 0 to 4.5 mT affects the floating potential drastically where an increase from −12.4 to −19.0 V is observed when the coil is initially turned on. Further increase of the magnetic field to 4.5 and 8.5 mT results in a decrease in V_f from −17.9 to −11.8 V. Information on other electron properties can be found in the supplementary information (Fig. S4).

The ion flux density (J_i) was calculated from the ion saturation current density (J_{sat}) using equation (2),

$$J_{sat} = eJ_i \tag{2}$$

where e is the charge of the electron. J_{sat} was in turn obtained from the I–V curves of the flat probe. An error of ~10% can be expected for the ion flux density. Fig. 3 shows the ion flux and ion energy as a function of the coil magnetic field. The ion flux exhibits an increasing trend around the substrate as the coil magnetic field is increased. At the highest magnetic field of 8.5 mT, J_i is increased by an order in comparison to when the coil is turned off at (0 mT). The ion energies (E_i) were calculated using equation (3),

$$E_i = e\left(V_{sub} - V_p\right) \tag{3}$$

where V_{sub} is the substrate potential. V_p is the plasma potential

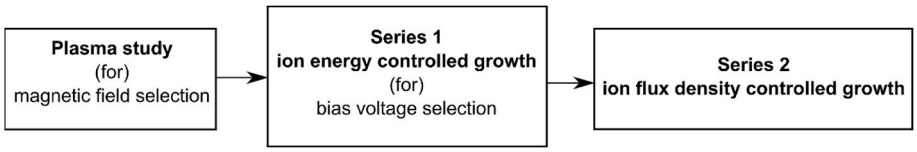

Fig. 1. Flow chart describing the order in which the work has been conducted and, results have been described.

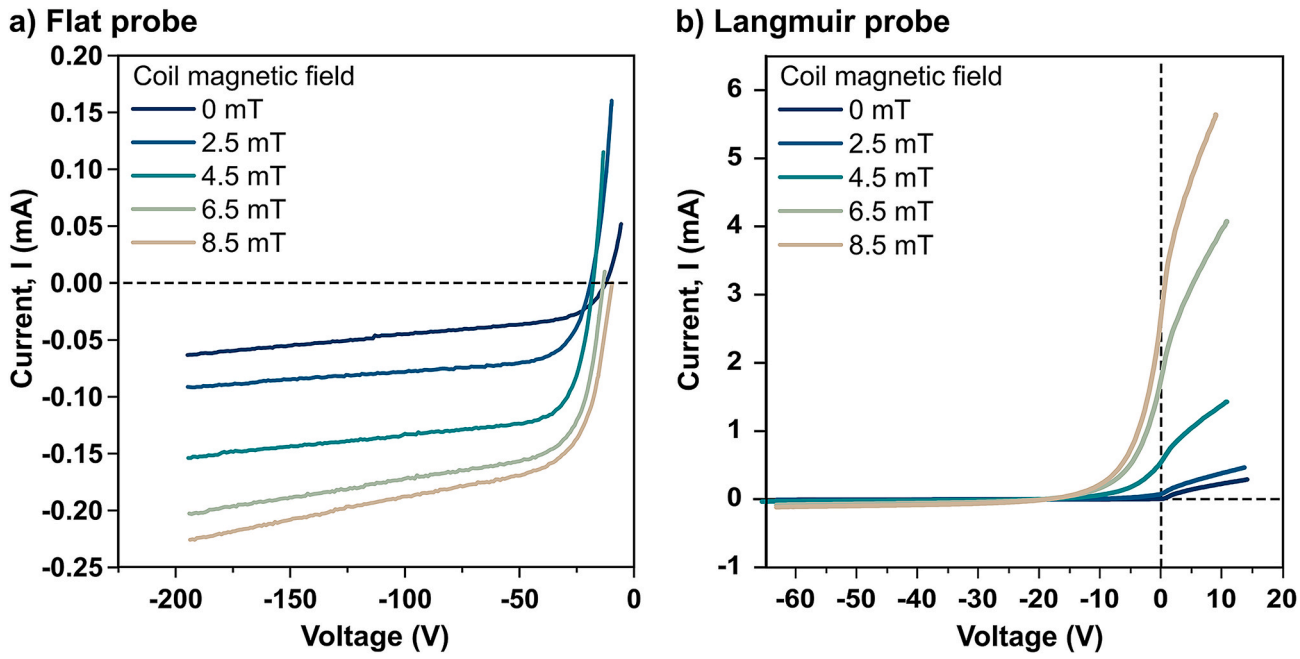

Fig. 2. I–V characteristics acquired with coil magnetic fields of 0–8.5 mT from a flat probe (a) and Langmuir wire probe (b), respectively.

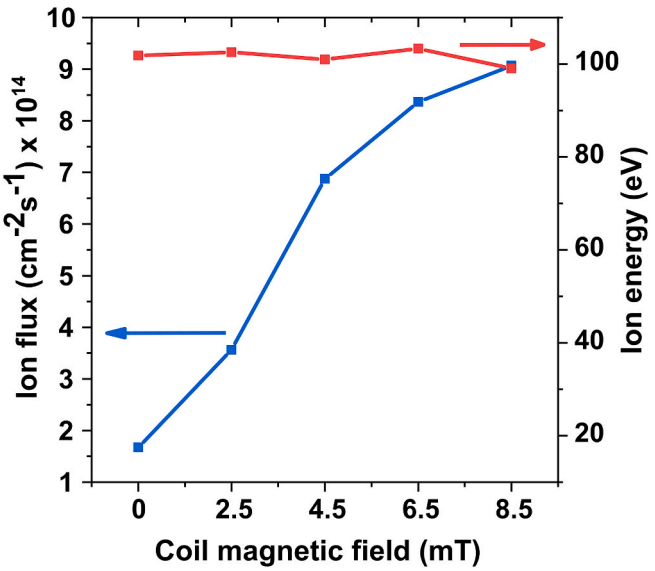

Fig. 3. Ion flux (Ji) and ion energies (E_i) were calculated considering the negative applied substrate bias of 100 V using equation (2).

determined from the Langmuir wire probe *I–V* characteristics and was found to be in the range of 1–3 V. When a bias voltage of −100 V is applied to the substrate, the ion energies range between 100 and 103 eV, i.e., the ion energies are determined by the applied negative bias voltage and the plasma potential.

A few general conclusions can be made from the plasma study that motivate the deposition parameters chosen for the thin film growth. Higher magnetic field results in the plasma plume condensing in a smaller area on the substrate (refer to images in Ref.15). While higher magnetic fields do produce higher J_i at the substrate, they also result in higher stress and hence possible delamination. For these reasons, the films grown in series 1 were deposited with sufficient ion flux density near the substrate to achieve a high ion bombardment but without reaching a stress level for the film to delaminate, thus the magnetic field was set at 4.5 mT. This results in a ~7 times greater ion flux density at substrate in comparison to when there is no magnetic field assistance.

3.2. Film growth

The microstructure and crystallinity of the samples grown in series 1 and 2 are described in this section. In brief, all crystalline films show a NaCl B1 type structure (isotype of: CrN, ScN, TiN), which hereafter is referred to as MeN B1, where Me is the sum of all metals (Cr, Fe, Co, Ni).

3.2.1. Series 1: Ion-energy-controlled growth

As noted above, the bias voltage applied to the substrate determines the energies of the incident ions. The primary effects of increased ion energy can be accelerated nucleation in the initial stages of growth and re-sputtering of the deposited material in the later stages. This can in turn lead to a change in composition, crystal structure, texturing, and evolution of multiple phases [17,18]. In order to carry out a quick screening and selection of the ion energy, multilayers were grown where each layer was deposited with an increasing bias voltage. Here it is important to consider that the observations described are not solely due to the varying processes parameters. The fact that the growth is dependent on the structure of the underneath layer can also influence

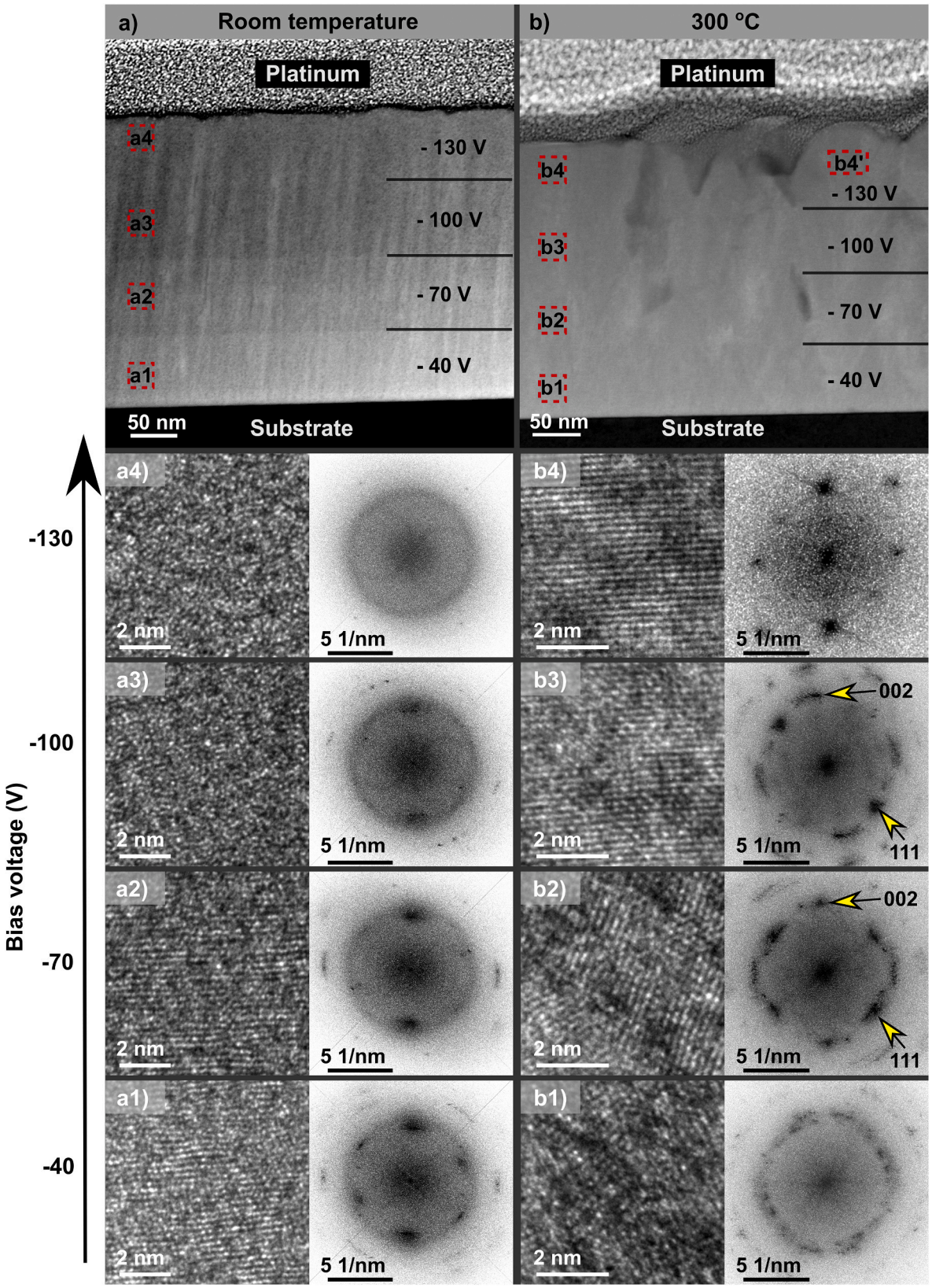

Fig. 4. Cross-section STEM image of (CrFeCoNi)N multilayered film grown at room temperature (a) and 300 °C (b), constant magnetic field of 4.5 mT and with bias voltage increasing from −40 V to −130 V. HRTEM images were acquired form the area enclosed in the red squares. (a1-4) HRTEM and corresponding FFT images of multilayered films deposited at room temperature, magnetic field of 4.5 mT and bias varied from −40 to −130 V. (b1-b4) HRTEM and corresponding FFT images of multilayered films deposited at a temperature of 300 C°, magnetic field of 4.5 mT and bias varied from −40 to −130 V. FFT corresponding to b4 taken from area enclosed in red box numbered 1on Fig. 4b.

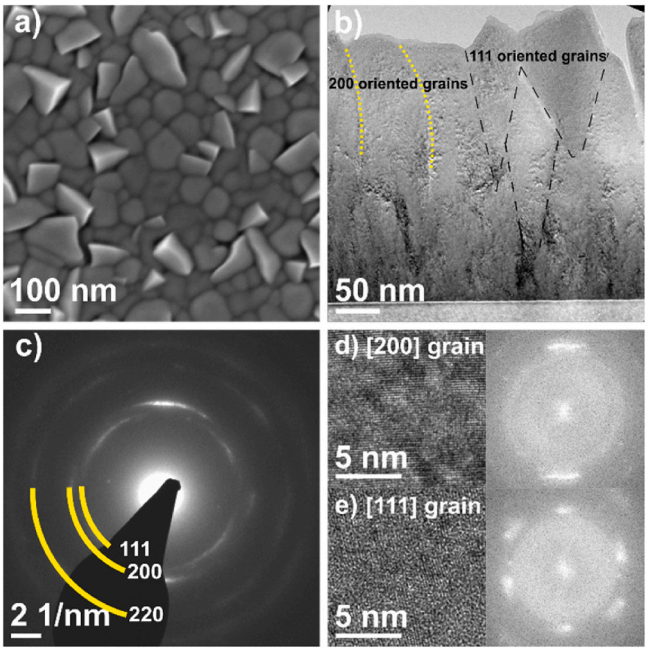

Fig. 5. a) Plan view SEM image of (CrFrCoNi)N multilayer film grown at 300 °C. b) Cross section TEM image depicting two grain orientations. Sample prepared by traditional polishing and ion milling. c) SAED pattern taken from bulk of the film cross section. (d) and (e) HRTEM images and corresponding FFT patterns taken from the 200 and 111 oriented two grains respectively.

the results. The multilayers are considered to be stochiometric nitrides although studies on CrN and VN films grown by dcMS and High-power impulse magnetron sputtering (HiPIMS) suggest that as the bias voltage is increased the nitrogen content in the film is decreased. This is due to the difference in binding energies [19,20]. No conclusion can be made in the case of the films in series 1 as Rutherford backscattering (RBS) results do not provide any information pertaining to the composition of the individual layers (see Supplementary Information Fig. S4) Fig. 4a shows the cross-section STEM image of the multilayered film grown at room temperature while changing the bias voltage. The coil magnetic field was fixed at 4.5 mT while the bias voltage was increased in steps from −40 to −130 V. Distinct layers are found which are overlayed on the columnar grains structure typical of physical vapor deposition (PVD) deposited thin films. The columns are seen to increase in width with the bias voltage from −40 to −130 V. A more pronounced effect of the bias voltage on the crystallinity of films can be observed in the high-resolution TEM (HRTEM) images and corresponding fast fourier transforms (FFT) (Fig. 4 a1- 4 a4). At lower bias voltages, the film grows steadily in a dense, columnar, crystalline MeN B1 structure oriented out of plane along the [011] zone axis. As the energy to the substrate is increased, the film grows with a 002 texture. Further increase of the bias voltage to – 100 V and higher results in Ar ion etching which may promote the formation of defects. For example, for the growth of TiN films, densification is observed along with increasing defect concentration in the film when the ion energies are increased [21–23]. In the case of the Cantor alloy-based nitride films, it is possible that, the crystal structure is damaged due to the increased incorporation of defects as the ion energy is increased. Consequently, the films become amorphous/fine grained in nature.

When the additional parameter of substrate temperature is introduced, the overall mechanism is more complex to understand as the total energy brought to the substrate is higher. Fig. 4b shows the cross-sectional STEM image of the multilayer grown at a higher deposition temperature (300 °C) while changing the bias voltage (−40 to −130 V). The complexity is already seen when comparing the FFT patterns of the multilayer grown at room temperature and 300 °C (see right images in Fig. 4a1 and 4b1), where the increase in deposition temperature promotes the crystallization of smaller grains with multiple orientations as indicated by more spots in the FFT pattern. From the overview for the cross-section STEM image of the film grown at 300 °C (Fig. 4b), the individual layers are not clearly seen however a change in the grain growth is observed. The individual layers display a competitive growth where the column width is seen to increase as the bias voltage is increased from −40 to −130 V. The selected area diffraction patterns (SAED) acquired from the bulk of the film in cross-section direction indicate that the films display a NaCl B1 type structure (Fig. 5c). The HRTEM (Fig. 4b1-4b4) and corresponding FFT's taken from the regions marked in red give us more information regarding the crystallinity of the film. At lower ion energies, the film exhibits a dense randomly oriented polycrystalline structure as evidenced by the HRTEM image (Fig. 4b1) and corresponding FFT. When the bias voltage is increased to −70 V the FFT shows an increase in the crystallinity with the occurrence of reflection from the (111) and (200) planes (Fig. 4b1 and corresponding FFT) of the MeN B1 structure. As the bias voltage is further increased the reflection from these plains become well defined suggesting the coarsening of grains (Fig. 4b3 and corresponding FFT). At the highest bias voltage of −130 V the majority of the grains display a 200 texture with. high crystallinity and visibly larger grains. When the ion energy is large enough, ion-atoms interactions cause the atoms to re-sputter and form adatom clusters on the surface of the films [24]. In this case these clusters crystallize with a 200 texture that can be observed in the surface images of the multilayer film grown at 300 °C (see Fig. 5a). A closer inspection of the TEM micrographs (Fig. 5b) shows that the (111) oriented grains originate from the first layer.

Table 3
Composition of monolithic (CrFrCoNi)N *films in series 2, grown at room temperature while increasing magnetic field from 0 - 6.5* mT *estimated by ToF-ERDA.*

Room temperature					
Magnetic field (mT)	Total metal (±1 at. %)	Nitrogen (±1 at. %)	N/Me ratio (±0.04)	Argon (±1 at. %)	Oxygen
0	49.5	49.8	1.01	0.7	<0.1%
2.5	46.6	52.0	1.12	1.4	
4.5	47.0	51.6	1.10	1.4	
6.5	46.3	53.3	1.15	0.4	
		300 °C			
0	53.4	46.5	0.87	0.1	<0.1%
2.5	52.9	46.9	0.89	0.2	
4.5	50.2	49.6	0.99	0.2	
6.5	49.5	50.2	1.01	0.3	

The structural analysis of the films in series 1 demonstrates the effects of ion energy over the effect of the ion flux density. The multilayer grown at room temperature becomes completely amorphous when the energy of ions bombarding the films is high, while the multilayer grown at 300 °C remains crystalline (bias voltage greater than −100 V, ion energies >100 eV). We see a transition in terms of crystallinity occurring in both temperatures when the ion energy is ~100 eV. This point of transition would be an interesting starting point to study the effects of the ion flux density on film growth. Therefore, the films in series 2 were grown with a constant ion energy of ~100 eV while gradually incrementing the ion flux density from ~1.5×10^{14} to ~8.5×10^{14} $cm^{-2}s^{-1}$.

3.2.2. *Series 2: Ion-flux-density-controlled growth*

By maintaining the ion energy and increasing the flux, the density of Ar ions at the substrate increases. The effects on film growth can be a continuous etching and removal of lighter elements which leads to a change in composition and phase, increased surface kinetics leading to stabilization of new phases or texturing of the films and a change in the residual stresses of the films. Table 3 gives the composition of the films grown at room temperature and 300 °C. The deposition rate of the films showed no particular trend and remained between 4 and 4.6 nm/min.

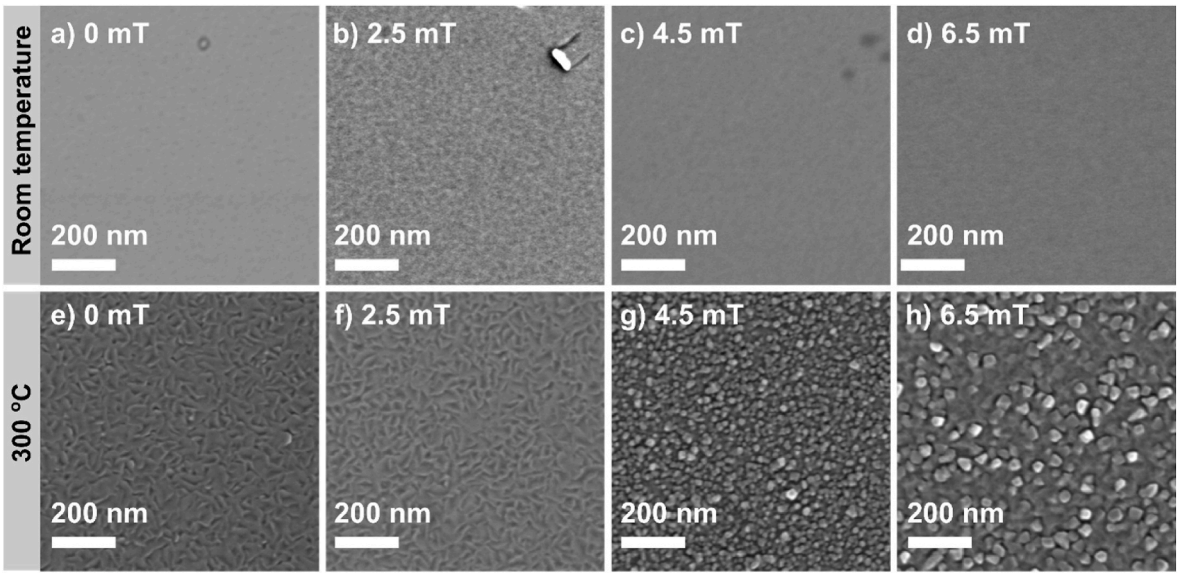

Fig. 6. SEM micrographs of (CrFeCoNi)N films in Series 2 grown at room temperature while keeping the bias voltage at constant at −100 V and varying the magnetic field from 0 to 6.5 mT (a–d) and (e–h) (CrFeCoNi)N films grown at higher deposition temperature with same processes parameters.

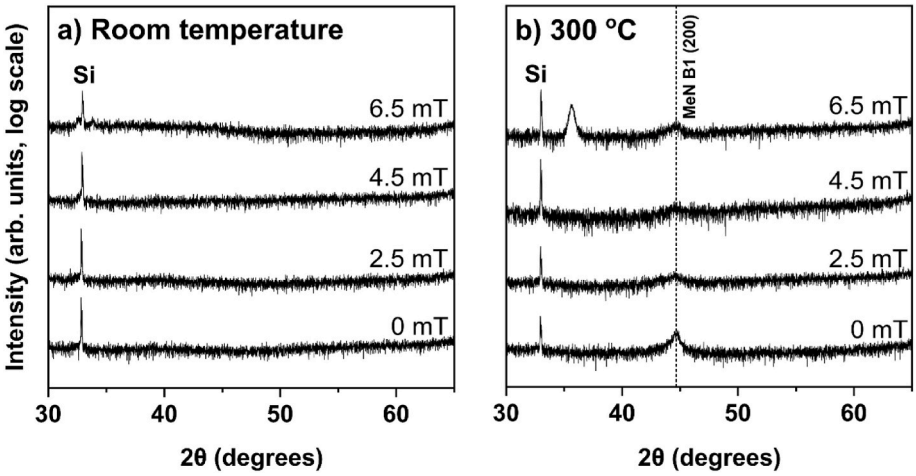

Fig. 7. XRD diffractograms of series 2 a) (CrFeCoNi)N films grown at room temperature while keeping the bias voltage at constant at −100 V and varying the soenoid coil magnetic field from 0 to 6.5 mT and (b) (CrFeCoNi)N films grown at higher depositon temperature with same processes paramaters.

From Table 3 we observe that the change in N/Me ratio is similar for both room temperature depositions and high temperature. The trends in composition change are however different. In the case of the room temperature films, when the magnetic field is at 0 mT the films are stochiometric nature. As the magnetic field is increased the films become over stochiometric. The films grown at higher temperature show a different trend where without the assistance of the magnetic field the films are under-stochiometric in nature and become stochiometric as the magnetic field is increased.

Fig. 6 shows the SEM micrographs of the films in series 2. The films grown at room temperature while increasing the magnetic field do not show any distinct features. The films grown at higher temperature, however, show a change in the surface morphology with increasing ion flux. The film grown without the assistance of the coil shows a scale like morphology. A similar morphology is seen when the coil is turned on to produce a magnetic field of 2.5 mT. As the magnetic field is increased to 4.5 mT and further, a change in the morphology is observed. The grains are more symmetrical and rounder in nature.

Fig. 7a shows the X-ray diffractograms of the films grown at room temperature while increasing the magnetic field at the substrate. The films do not show any diffraction peaks and appear X-ray amorphous irrespective of the ion flux during growth. X-ray diffractograms of the films grown at 300 °C are presented in Fig. 7b. The higher temperature initiates crystallization of the film. When the magnetic field is 0 mT a single peak is observed corresponding to the 200 reflection of a MeN B1 phase with a lattice parameter of 4.06 ± 0.02 Å. This trend continues as the magnetic field is increased however the peak intensity is reduced which may indicate a decrease in concentration of the particular phase. When the magnetic field is at 6.5 mT, the film starts to show the effects of the increased ion flux. A peak at 35.6° appears in the x-ray diffractogram which does not correspond to the 111 reflection of the MeN B1 and hence may be considered to belong to a secondary phase. This is confirmed not only from the θ-2θ scans but also from grazing incidence angle XRD (GIXRD) (see Supplementary Information Fig. S6, Fig. S7 and Table S1) and SAED patterns (Fig. 8).

These result may seem a bit surprising since studies on ion assisted film growth of TiN demonstrated that the increased flux of ions at the substrate alters the surface kinetics of the metal atoms and influences the texture [25–28].

Here, when the ion flux density is low, the multicomponent films

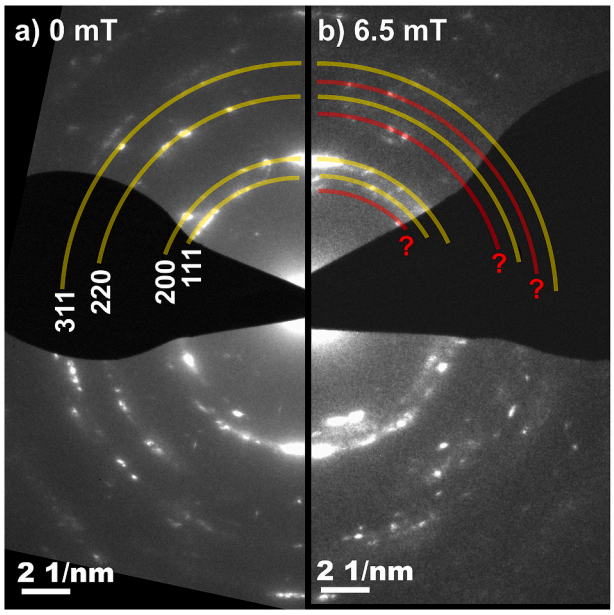

Fig. 8. SAED pattern taken from the (CrFrCoNi)N film cross-sections. (a) film grown at 300 °C without the coil. Diffused spots correspond to the $MeN_{1-\delta}$ B1structure with lattice parameter of 4.06 ± 0.02 Å. (b) film grown at 300 °C with the magnetic field set at 6.5 mT. Rings marked in red correspond to the cubic phase with lattice parameter of 4.42 ± 0.02 Å.

have a structure similar to the NaCl structure of CrN where Cr in the lattice is mostly replaced by, Fe, Co, Ni with a smaller atomic radius than Cr. CrN has a lattice parameter of approximately 4.13 Å (ICDD reference code: 01-074-8390). In the case of the multicomponent films, at lower ion flux density the films are understoichiometric and have a NaCl-like structure with a lattice parameter smaller than CrN ($MeN_{1-\delta}$ B1- 4.06 Å). This substoichiometric $MeN_{1-\delta}$ phase appears regardless of coil magnetic field, with the same cell parameter. As the ion flux density is increased, the N_2^+ ion concentration at the substrate is also increased resulting in a stochiometric composition but with the appearance of the secondary phase (Fig. 8b, Table 3).

From XRD, GIXRD and SAED patterns, the detected reflections could be assigned to a cubic material system which is should be rich in nitrogen due to the overall composition of the film (Me/N = 1). The lattice parameter of this cubic phase determined from BB-XRD, GIXRD and TEM was 4.42 Å (See supplementary information, Table S1).

4. Conclusion

We have investigated the effects of ion energy and ion flux density on multicomponent CrFeCoNi nitride films. The ion flux density at the substrate was controlled by applying a magnetic field at substrate position. At room temperature, the films became increasingly amorphous when the ion energy increased (−40 eV to −130 eV), while the ion flux density had no significant effect on the crystallinity or morphology of the films. For the films grown at 300 °C, the higher ion energy promotes the crystallization of larger grains and multiple orientations. The ion flux density influences the morphology, composition, and phase formation in the multicomponent films. Higher ion flux results ($>6 \times 10^{14}$ $cm^{-2}s^{-1}$) in the increased nitrogen incorporation in the films. Magnetic-field-assisted growth technique can be used to control the structure of multicomponent nitrides without compromising the deposition rate.

Since Cantor alloy-based thin films are finding applications as hard, wear-resistant, corrosion and oxidation-resistant coatings, what is needed is a fundamental understanding of the material system and strategies to improve film properties. The results presented in this paper could serve as a guideline for understanding the effect of energetic particle bombardment in Cantor alloy-based systems for future studies using HiPIMS.

CRediT authorship contribution statement

Smita G. Rao: Writing – original draft, Investigation, Formal analysis, Data curation, Conceptualization. **Rui Shu:** Investigation, Formal analysis. **Robert Boyd:** Investigation, Formal analysis. **Arnaud le Febvrier:** Writing – review & editing, Supervision, Investigation, Formal analysis, Conceptualization. **Per Eklund:** Writing – review & editing, Supervision, Project administration, Funding acquisition, Conceptualization.

Declaration of competing interest

The authors declare that they have no known competing financial interests or personal relationships that could have appeared to influence the work reported in this paper.

Data availability

Data will be made available on request.

Acknowledgments

The work was supported financially by the VINNOVA Competence Centre FunMat-II (grant no. 2016-05156), the Swedish Government Strategic Research Area in Materials Science on Functional Materials at Linköping University (Faculty Grant SFO-Mat-LiU No. 2009 00971), the Knut and Alice Wallenberg foundation through the Wallenberg Academy Fellows program (KAW-2020.0196) and the Swedish Research Council (VR) under project number 2021-03826. Accelerator operation was supported by Swedish Research Council VR-RFI (Contract No. 2019-00191). Daniel Primetzhofer and Gyula Nagy from Uppsala University, Sweden are acknowledged for their assistance in the ERDA and RBS measurements.

Appendix A. Supplementary data

Supplementary data to this article can be found online at https://doi.org/10.1016/j.vacuum.2022.111331.

References

[1] I. Petrov, L. Hultman, J.-E. Sundgren, J.E. Greene, Polycrystalline TiN films deposited by reactive bias magnetron sputtering: effects of ion bombardment on resputtering rates, film composition, and microstructure, J. Vac. Sci. Technol. A Vacuum, Surfaces, Film. 10 (1998) 265, https://doi.org/10.1116/1.578074.
[2] D.M. Mattox, Particle bombardment effects on thin-film deposition: a review, J. Vac. Sci. Technol. A Vacuum, Surfaces, Film. 7 (1989) 1105–1114, https://doi.org/10.1116/1.576238.
[3] F.A. Smidt, Use of ion beam assisted deposition to modify the microstructure and properties of thin films, Int. Mater. Rev. 35 (1990) 61–128, https://doi.org/10.1179/095066090790323975.
[4] U. Helmersson, M. Lattemann, J. Bohlmark, A.P. Ehiasarian, J.T. Gudmundsson, Ionized physical vapor deposition (IPVD): a review of technology and applications, Thin Solid Films 513 (2006) 1–24, https://doi.org/10.1016/J.TSF.2006.03.033.
[5] I. Petrov, F. Adibi, J.E. Greene, L. Hultman, J.E. Sundgren, Average energy deposited per atom: a universal parameter for describing ion-assisted film growth? Appl. Phys. Lett. 63 (1998) 36, https://doi.org/10.1063/1.109742.
[6] I. Petrov, L. Hultman, U. Helmersson, J.E. Sundgren, J.E. Greene, Microstructure modification of TiN by ion bombardment during reactive sputter deposition, Thin Solid Films 169 (1989) 299–314, https://doi.org/10.1016/0040-6090(89)90713-X.
[7] I. Ivanov, P. Kazansky, L. Hultman, I. Petrov, J.-E. Sundgren, Influence of an external axial magnetic field on the plasma characteristics and deposition conditions during direct current planar magnetron sputtering, J. Vac. Sci. Technol. A Vacuum, Surfaces, Film. 12 (1994) 314–320, https://doi.org/10.1116/1.578874.
[8] C. Engström, T. Berlind, J. Birch, L. Hultman, I.P. Ivanov, S.R. Kirkpatrick, S. Rohde, Design, plasma studies, and ion assisted thin film growth in an unbalanced dual target magnetron sputtering system with a solenoid coil, Vacuum 56 (2000) 107–113, https://doi.org/10.1016/S0042-207X(99)00177-3.

[9] K.H. Müller, Model for ion-assisted thin-film densification, J. Appl. Phys. 59 (1998) 2803, https://doi.org/10.1063/1.336960.
[10] L. Hultman, J.-E. Sundgren, L.C. Markert, J.E. Greene, Ar and excess N incorporation in epitaxial TiN films grown by reactive bias sputtering in mixed Ar/N2 and pure N2 discharges, J. Vac. Sci. Technol. A Vacuum, Surfaces, Film. 7 (1998) 1187, https://doi.org/10.1116/1.576251.
[11] D.B. Miracle, O.N. Senkov, A critical review of high entropy alloys and related concepts, Acta Mater. 122 (2017) 448–511, https://doi.org/10.1016/j.actamat.2016.08.081.
[12] E.P. George, D. Raabe, R.O. Ritchie, High-entropy alloys, Nat. Rev. Mater. 48 (4) (2019) 515–534, https://doi.org/10.1038/s41578-019-0121-4, 2019.
[13] J.-W. Yeh, S.-K. Chen, S.-J. Lin, J.-Y. Gan, T.-S. Chin, T.-T. Shun, C.-H. Tsau, S.-Y. Chang, Nanostructured high-entropy alloys with multiple principal elements: novel alloy design concepts and outcomes, (n.d.). https://doi.org/10.1002/adem.200300567.
[14] A. le Febvrier, L. Landälv, T. Liersch, D. Sandmark, P. Sandström, P. Eklund, An upgraded ultra-high vacuum magnetron-sputtering system for high-versatility and software-controlled deposition, Vacuum (2021), 110137, https://doi.org/10.1016/j.vacuum.2021.110137.
[15] J. Overman, Design and Implementation of Automated Plasma Probe, Linköping University, 2000.
[16] K. Arstila, J. Julin, M.I. Laitinen, J. Aalto, T. Konu, S. Kärkkäinen, S. Rahkonen, M. Raunio, J. Itkonen, J.P. Santanen, T. Tuovinen, T. Sajavaara, Potku - new analysis software for heavy ion elastic recoil detection analysis, Nucl. Instrum. Methods Phys. Res. Sect. B Beam Interact. Mater. Atoms 331 (2014) 34–41, https://doi.org/10.1016/j.nimb.2014.02.016.
[17] M. Marinov, Effect of ion bombardment on the initial stages of thin film growth, Thin Solid Films 46 (1977) 267–274, https://doi.org/10.1016/0040-6090(77)90182-1.
[18] T. Takagi, Ion–surface interactions during thin film deposition, J. Vac. Sci. Technol. A Vacuum, Surfaces, Film. 2 (1998) 382, https://doi.org/10.1116/1.572748.
[19] H. Hajihoseini, M. Kateb, S. Ingvarsson, J.T. Gudmundsson, Effect of substrate bias on properties of HiPIMS deposited vanadium nitride films, Thin Solid Films 663 (2018) 126–130, https://doi.org/10.1016/J.TSF.2018.06.060.
[20] Q. Kong, L. Ji, H. Li, X. Liu, Y. Wang, J. Chen, H. Zhou, Influence of substrate bias voltage on the microstructure and residual stress of CrN films deposited by medium frequency magnetron sputtering, Mater. Sci. Eng. B. 176 (2011) 850–854, https://doi.org/10.1016/J.MSEB.2011.04.015.
[21] L. Hultman, J.E. Sundgren, J.E. Greene, D.B. Bergstrom, I. Petrov, High-flux low-energy (≈20 eV) N+2 ion irradiation during TiN deposition by reactive magnetron sputtering: effects on microstructure and preferred orientation, J. Appl. Phys. 78 (1998) 5395, https://doi.org/10.1063/1.359720.
[22] I. Petrov, A. Myers, J.E. Greene, J.R. Abelson, Mass and energy resolved detection of ions and neutral sputtered species incident at the substrate during reactive magnetron sputtering of Ti in mixed Ar+N 2 mixtures, J. Vac. Sci. Technol. A Vacuum, Surfaces, Film. 12 (1994) 2846–2854, https://doi.org/10.1116/1.578955.
[23] I. Petrov, P.B. Barna, L. Hultman, J.E. Greene, Microstructural evolution during film growth, J. Vac. Sci. Technol. A Vacuum, Surfaces, Film. 21 (2003) S117–S128, https://doi.org/10.1116/1.1601610.
[24] W. Ensinger, Low energy ion assist during deposition - an effective tool for controlling thin film microstructure, Nucl. Instruments Methods Phys. Res. Sect. B Beam Interact. Mater. Atoms 127–128 (1997) 796–808, https://doi.org/10.1016/S0168-583X(97)00010-4.
[25] I. Petrov, F. Adibi, J.E. Greene, L. Hultman, J.E. Sundgren, Average energy deposited per atom: a universal parameter for describing ion-assisted film growth, Appl. Phys. Lett. 63 (1993) 36–38, https://doi.org/10.1063/1.109742.
[26] J.E. Greene, Epitaxial crystal growth by sputter deposition: applications to semiconductors. part 1, Crit. Rev. Solid State Mater. Sci. 11 (1983) 47–97, https://doi.org/10.1080/01611598308243645.
[27] J.E. Gerbi, J.R. Abelson, Low temperature magnetron sputter deposition of polycrystalline silicon thin films using high flux ion bombardment, J. Appl. Phys. 101 (2007), https://doi.org/10.1063/1.2710301, 0–5.
[28] B. Strickland, C. Roland, Low-temperature growth and ion-assisted deposition, Phys. Rev. B 51 (1994) 15–1995.